This article has been accepted for publication in a future issue of this journal, but has not been fully edited. Content may change prior to final publication. Citation information: DOI 10.1109/TSTE.2019.2898115, IEEE Transactions on Sustainable Energy

A Single Input Variable FLC for DFIG Based WPGS in Standalone Mode

Sambasivaiah Puchalapalli, *Member, IEEE*, and Bhim Singh, *Fellow, IEEE*

***Abstract*--This paper proposes a novel single input variable fuzzy logic controller (FLC) strategy for a wind turbine driven doubly fed induction generator (DFIG) with a battery energy storage (BES) in autonomous mode. The proposed control scheme has multi-functionalities such as harmonic elimination, compensation of unbalanced load currents and extraction of maximum power from the wind. The control of rotor side converter and load side converter, is based on field oriented approach. The proposed single input variable FLC based control has good dynamic response as compared to conventional control algorithms. The tip speed ratio based maximum power point tracking technique is used to extract maximum power from the wind. The simulation of DFIG based wind power generation system (WPGS) is carried out under various conditions such as constant wind speed, variable wind speeds and load currents unbalancing using Simpower Systems toolbox of MATLAB. The DFIG stator voltages and currents are found balanced and sinusoidal by maintaining constant frequency and voltage at PCC. Finally, a prototype of DFIG based wind energy system is developed in the laboratory to verify the performance of the proposed control scheme at variable wind speeds and linear, nonlinear loads. The total harmonic distortions of the DFIG stator voltages and currents are obtained within limits of the IEEE 519 standard.**

***Index Terms*--Wind power generation system (WPGS), DFIG, battery energy storage (BES), fuzzy logic control (FLC), MPPT.**

NOMENCLATURE

v_{sa}, v_{sb}, v_{sc}	Stator voltages
i_{sa}, i_{sb}, i_{sc}	Stator currents
i_{La}, i_{Lb}, i_{Lc} and i_{Ln}	Load currents and neutral current
i_{ra}, i_{rb}, i_{rc}	rotor currents
C_{dc}, L_f	DC link capacitance, interfacing inductance
V_b, V_{dc}	Battery nominal voltage, DC link voltage
V_w, P_m, C_p	Wind speed, power captured by the wind turbine, coefficient of wind turbine
ρ, β, λ, r, η, ω_T	Air specific density, blade pitch angle, tip speed ratio, radius of wind turbine, gear ratio, angular speed of wind turbine
ω_r, λ_{opt}, ω^*_r	DFIG rotor speed, optimal tip speed ratio, reference rotor speed of DFIG
P_{rin}, P_{rs}, P_{rr}	DFIG total power, rated stator power, rated rotor power
s_{rp}, V_{rm}, m	Slip at rated power, rotor maximum voltage, modulation index
$V_{L(LV)}$	Voltage at low voltage (LV) side of transformer
VA_{LSC}	Volt-ampere rating of load side converter (LSC)
$I_{r(LSC)}$	Current rating of LSC
$I_{IGBT(LSC)}$	Current rating of insulated gate bipolar transistor (IGBT) of LSC
I_{pLSC}, I_{ppr}	LSC peak current, peak-peak current ripple of LSC
V_{dcm}, a, f_{sw}	Maximum DC bus voltage, safety factor, switching frequency
Q_{rr}	Rated rotor reactive power
$VA_{(RSC)}$, $I_{r(RSC)}$	Rotor side converter (RSC) volt-ampere rating, current rating of RSC
I_{pRSC}, $I_{IGBT(RSC)}$	RSC peak current, current rating of IGBT of RSC
i_{dr}, i_{qr}	Direct and quadrature axes component of rotor currents
ϕ_{sd}, p	Stator flux, number of poles
$K_{p\omega}$, $K_{i\omega}$	Proportional and integral gain constants of speed controller
e_ω, $e_{r\omega}$, γ_ω	Speed error, rate of change of speed error and speed error distance of fuzzy logic controller (FLC)
i^*_{dr}, i^*_{qr}	Reference direct and quadrature axes component of rotor currents
I_{mr}, X_m	Magnetizing current and magnetizing reactance of DFIG
V_t, V^*_t	Actual and reference terminal voltages
θ_{sp}, θ_r, θ_f, ω_0	Slip angle, sensed rotor angle, fixed electrical angle, angular base frequency
i^*_{ra}, i^*_{rb}, i^*_{rc}	Reference rotor currents
e_v, γ_v, K_{pv}, K_{iv}	Voltage error, voltage error distance of FLC, proportional and integral constants of voltage controller
i^*_{ds}, i^*_{qs}	Reference direct and quadrature axes component of stator currents
i^*_{sa}, i^*_{sb}, i^*_{sc}	Reference stator currents
f_s	Stator frequency
P_s, P_{LSC}, P_L, P_b	Stator power, LSC power, load power and battery power

Sambasivaiah Puchalapalli and Bhim Singh are with the Department of Electrical Engineering, Indian Institute of Technology Delhi, New Delhi-110016, India (e-mail:sambasivaiah8888@gmail.com and bhimsinghiitd61@gmail.com)

I. INTRODUCTION

Owing to usage of fossil fuel for power generation, some adverse effects are observed on the environment such as greenhouse gas, acid rain, ozone layer depletion and global warming [1]. To balance between power generation and power consumption, a domestic power generation must be initiated in

This article has been accepted for publication in a future issue of this journal, but has not been fully edited. Content may change prior to final publication. Citation information: DOI 10.1109/TSTE.2019.2898115, IEEE Transactions on Sustainable Energy

the distribution network to keep the climate clean and to feed the local loads. Nowadays, the policies for renewable power generation support the capital subsidies to promote its applications and to provide subsidies in taxes [2]. The usage of renewable energy sources (RES) in the distribution system, is booming in the developing countries due to market penetration, learning skill and emerging technologies. Nowadays, small scale RES are installed in household buildings, commercial buildings, irrigations, industries, healthcare services, etc. Moreover, some advantages of RES, are mentioned as follows.

- Renewable power generation is eco-friendly as it generates no waste during operation and having negligible contribution in greenhouse effects, acid rains etc. Therefore, green energy sources are pollution free and have minimal impact on the environment.
- The RES has low operating cost, low maintenance cost as it is freely available with inexhaustible natural resource.

Among the renewable energy sources, the researchers have found the increased attention toward wind energy because of advancements in wind turbines and in view of economic aspects [3]-[5]. Wind turbines are categorized predominantly as fixed and variable speed types. Earlier fixed speed wind turbines have been used because of their secure and comfortable operating features, but noticeable quantity of power is wasted in the same [6]. Therefore, there has been expanded attention towards the doubly fed induction generator (DFIG) coupled to varying speed wind turbines all over the globe. The use of DFIG with wind turbine, has many advantages as compared to topologies with constant speed generators as mentioned in [7], [8] as,

- The rating of the converter is reduced because it carries only slip times the stator power.
- The DFIG is highly energy efficient and has less power losses.
- It produces less acoustic noise.
- Most importantly, it is highly suitable for variable speed operation, which is required to obtain peak power, especially during varying wind conditions.

Standalone and grid connected modes of operation, are feasible with wind turbine coupled DFIG, in a wind power generation system (WPGS). Notable research has been carried out on the grid connected DFIG based WPGS [7], [8]. In [7], the control of grid power flow, is not effective as there is no load side converter is installed with DFIG. Moreover, the power quality aspects with respect to the utility, are not analyzed in the same. The model predictive controller based strategy has been analyzed in [8] for DFIG under distorted grid voltages. However, it has high computational burden, high complexity and high memory requirement. A sliding mode based control scheme has been described in [9] for weak grid voltages. The life time of the VSC, is reduced as sliding mode controller generates hard switching pulses.

However, the amount of research on standalone DFIG based WPGS is not prominent and explored. In standalone mode of operation, it is very crucial to maintain constant frequency, constant voltage at load end along with the harmonics within the permissible limits [10]. The control schemes for both rotor side converter (RSC) and load side converter (LSC) of DFIG, are modeled such that the aforementioned objectives are attained.

There are various maximum power point tracking (MPPT) techniques in the literature [11], [12] to acquire peak power from the wind. However, tip speed ratio MPPT method is used in this work. The battery energy storage (BES) plays a key role in particular with standalone mode of operation of DFIG. It is because, lower demand at high wind speeds, drives the surplus power towards BES for charging. Similarly if the load demand is high and wind speed is low, then BES supplies the balance power such that the wind turbine generator operates at MPPT. Some of the literature for standalone operation of DFIG with BES is found in [13], [14]. Mendis *et al.* [13] have analyzed standalone DFIG with BES connected at DC link through buck boost bidirectional converter. However, many proportional integral controllers (PICs) make the control algorithm of overall system complex and also, it lacks the experimental validation. Cardenas *et al.* [14] have presented sensorless operation of DFIG in standalone mode though BES is not used. In the literature [14], the absence of a battery in standalone system, causes the DC link voltage to rise to high value, which needs to be avoided and also the control is complex due to more PICs. Goel *et al.* [15] have presented standalone DFIG with BES attached to common DC link of two voltage source converters (VSCs) connected back to back in the rotor circuit. Naidu *et. al.* [16] have demonstrated the performance of DFIG in standalone mode with and without BES. However, the tracking of voltage reference and speed reference, is done by the use of PICs within the control. Many control schemes in the literature, are having at least two PICs. The tuning of the PICs in dynamic scenario, is prone to the system performance and also vulnerable to capture peak power out of the wind in DFIG-based WPGS. Therefore, researchers have started implementing fuzzy logic tuned PICs for DFIG based WPGS [17], [18]. The conventional fuzzy logic controller (FLC) contains the large set of rules, which increases the computational burden and memory requirement etc. The system behaviour in transient conditions, is affected because of lack of tuning PICs [17]. Therefore, a single input variable tuned PIC, is described in [19] to avoid earlier mentioned issues. The distance between origin and error vectors, are inputs to the FLC. The certain benefits of a single input variable fed FLC, are given in [19].

With improvements in the battery energy storage technology, standalone WPGS plays vital role where grid extension is very costly. The grid outage is also very common issue, particularly in the remote windy regions. The standalone WPGS for street light, telecommunication stations, sign boards etc., have been analysed in [20].The off-grid solution for remotely located areas, are analyzed in the literature [21]. The optimal solution for WPGS with energy storage system, has been described in [22] for remotely located community.

The essential contribution of this study, consists of salient characteristics of the control algorithms, which are as follows.

This article has been accepted for publication in a future issue of this journal, but has not been fully edited. Content may change prior to final publication. Citation information: DOI 10.1109/TSTE.2019.2898115, IEEE Transactions on Sustainable Energy

- The single input variable fed FLC is used to tune PIC of terminal voltage at PCC by using LSC and PIC of speed control for MPPT operation using RSC, which has less computational burden and memory requirement.
- Both RSC and LSC control algorithms are developed using stator flux oriented approach.
- The energy storage device is directly attached at DC link of two VSCs connected back to back, which helps in storing and providing balance power in dynamic operating conditions of DFIG based WPGS.
- The DFIG stator currents, PCC voltages are balanced and sinusoidal, which have the harmonics within the IEEE-519 standard.
- The terminal voltage at PCC and its frequency, are maintained constant during dynamic conditions such as variable wind speed, load unbalancing etc.

The DFIG based WPGS in standalone mode feeding three-phase, four wire loads, is modelled and simulated using SimPowerSystems tool box of MATLAB. The reasons behind the not connecting neutral wire to the stator of the doubly fed induction generator (DFIG) are as follows. The generator currents are sinusoidal and balanced, which are always taken care by the control of load side converter (LSC). Moreover, the neutral wire is required to deliver power to the single phase loads (examples: house loads, commercial loads, small scale industrial loads) and imbalanced local loads. In the proposed system, the transformer provides neutral wire to deliver power to the aforementioned type of imbalanced and single phase loads. In the proposed topology, the load side converter supplies the non-fundamental components and imbalanced components of local loads, which are connected at point of common coupling. Moreover, for the protection point of view, the power generation system in the power plant, is three-phase three-wire to generate balanced power [23-24]. The peak power from the wind, is obtained by employing tip speed ratio MPPT technique. Using a developed prototype, the steady state and transient performances are analyzed in detail.

II. System Configuration and its Component Design

Fig. 1 shows the DFIG based WPGS, which is designed to deliver an average load of 2 kW and peak load of 4 kW in standalone mode of operation. The DFIG stator windings feed the load whereas, the rotor windings are fixed to PCC via two VSCs connected in back to back. The VSC, which is connected near PCC, is termed as LSC and the VSC that is connected to rotor winding is named as RSC. The BES is connected at common DC link of two VSCs as shown in Fig. 1. The design of each component in this system, is explored in the subsequent subsections.

A. Design of Wind Turbine and Gear Mechanism

The wind power captured by the turbine, P_m is given as [25],

$$P_m = 0.5C_p(\lambda,\beta)\rho A V_w^3 = 0.5C_p(\lambda,\beta)\rho\pi r^2 V_w^3 \quad (1)$$

where, ρ is air specific density, which is considered as 1.1514 kg/m^3; V_w denotes wind speed in (m/s); A is area occupied by the wind turbine blades in (m^2); C_p is called power efficiency or coefficient of turbine, whose value depends on blade pitch angle β in (deg) and tip speed ratio λ; r is the radius of wind turbine in (m).

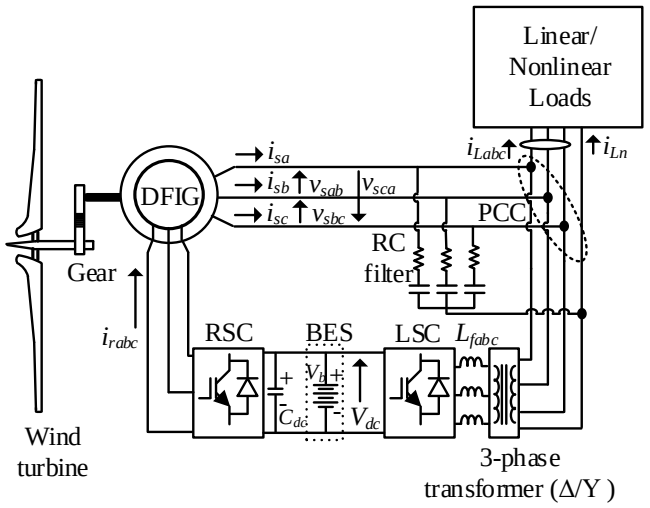

Fig. 1. DFIG based WPGS in standalone mode with BES.

The C_p is expressed in [25] as,

$$C_p(\lambda,\beta) = C_1\{(C_2/\lambda_i) - C_3\beta - C_4\}e^{-C_5/\lambda_i} + C_6\lambda \quad (2)$$

where, $\frac{1}{\lambda_i} = \frac{1}{\lambda + 0.08\beta} - \frac{0.035}{\beta^3 + 1}$

Moreover, the constants $C_1 = 0.5176$, $C_2 = 116$, $C_3 = 0.4$, $C_4 = 5$, $C_5 = 21$ and $C_6 = 0.0068$ are considered. The pitch angle of the blade is considered as $\beta = 0°$ and it is maintained at constant value.

The λ gives the relationship between wind speed and tip speed of blade as,

$$\lambda = \frac{\omega_T \times r}{V_w} \quad (3)$$

where, ω_T represents the rotational speed of a wind turbine.

In this work, a wind turbine of 4.81 kW, is designed at 12 m/s rated wind speed by considering step up gear mechanism. The design is such that C_p attains a maximum value of 0.48 and corresponding λ is of 8.1, which is considered to be optimum value for acquiring peak power from the available wind. The wind turbine radius is calculated from (1) is 1.8 m.

The DFIG rotor speed ω_r is expressed in terms of, ω_T and gear ratio η as,

$$\omega_r = \eta\omega_T \quad (4)$$

The minimum and maximum rotor speeds of DFIG, are taken as 110 rad/s and 204 rad/s. By (3) and (4), η is calculated as 3.77 at 12 m/s, rated wind speed and 204 rad/s, rotor speed.

B. Tip Speed Ratio Wind-MPPT Method

From the speed-power characteristics of wind turbine, it is evident that the rotor speed of DFIG has to vary to extract peak power out of available wind speed. The same is accomplished by generating suitable reference speed for a specific wind speed. In this work, the tip speed ratio MPPT method [16] is used. Moreover, its mathematical formulation

This article has been accepted for publication in a future issue of this journal, but has not been fully edited. Content may change prior to final publication. Citation information: DOI 10.1109/TSTE.2019.2898115, IEEE Transactions on Sustainable Energy

to derive the reference speed is as follows.
Using (4), the rotational speed of wind turbine is expressed as,

$$\omega_T = \frac{\omega_r}{\eta} \tag{5}$$

Substituting (5) in (3) result in as,

$$\lambda = \frac{\omega_r \times r}{\eta \times V_w} \tag{6}$$

In (6), for $\lambda = \lambda_{opt}$, ω_r gives the reference speed ω^*_r as,

$$\omega_r^* = \frac{\eta \times \lambda_{opt} \times V_w}{r} \tag{7}$$

By substituting the respective values in (7), the reference rotor speed is expressed in terms of V_w as,

$$\omega_r^* = \frac{3.77 \times 8.1 \times V_w}{1.8} \cong 17 \times V_w \tag{8}$$

C. Determination of Power Rating for DFIG

The DFIG is able to deliver power, both from the stator and rotor during super synchronous speed operation. Since speed range of the rotor, is considered between 110 rad/s to 204 rad/s, the corresponding slip is +30.0% and -30.0%, respectively. The DFIG is selected such that it delivers rated power at rated wind speed. At rated power condition, DFIG also delivers power from the rotor, which is slip times the stator power. The total amount of power delivered by DFIG P_{rin} is expressed in terms of rated stator power P_{rs} and rated rotor power P_{rr} as,

$$\left.\begin{aligned} P_{rin} &= P_{rs} + P_{rr} = P_{rs} + |s_{rp}|\,P_{rs} = (1+|s_{rp}|)P_{rs} \\ P_{rs} &= \frac{P_{rin}}{(1+|s_{rp}|)} \end{aligned}\right\} \tag{9}$$

where, s_{rp} represents the slip at rated power and it is -0.3. After substituting this value in (9), gives rated stator power P_{rs} of 3.7 kW. Therefore, it is admissible to design a DFIG with rating of 3.7 kW, because the need of reactive power is taken care by the RSC. This is the main advantage of DFIG.

D. Design of DC Link Voltage and BES

The rotor voltage attains a maximum value at a slip of 0.3, because slip times the stator voltage equals the rotor voltage. For a 415 V system, the rotor voltage is determined as, V_{rm} = $0.3 \times 415 \cong 125$ V. Thus, the DC link voltage V_{dc} is obtained with the following relation as,

$$V_{dc} \geq \left(\frac{2\sqrt{2}}{\sqrt{3} \times m}\right) V_{rm} \tag{10}$$

where, V_{rm} is the rotor maximum voltage; m is the modulation index, is selected as a unity. By substituting the values in (10), the DC link voltage is obtained as 204.1 V. In this system, it is selected as 240 V, which can be realized using 20 batteries of 12 V each.
As discussed earlier, the DFIG based WPGS is designed to supply for 30 hours at an average load of 2 kW. Hence, the storage capacity of BES turns out to be 60 kWh. The ampere-hour rating of BES, is calculated as (60 kWh/240) and comes to be 250 AH. Therefore, a 240 V, 250 AH BES is required for this system. In practice, a set of 12 V and 125 AH batteries are available, so to achieve 240 V, 20 batteries are connected in series and to obtain 250 AH rating, another 20 batteries are connected in parallel with the previous ones.

E. Design of Transformer and VSCs Rating

The system is designed for 3-phase, 4-wire distribution network, to cater single phase loads, for which a 3-phase transformer is used to provide a neutral point. Since the opted voltage of the battery is 240 V, the low voltage (LV) winding voltage, $V_{L(LV)}$ as per (10) should be less than 147 V and it is chosen to be 125 V. Therefore, a 5 kVA, 125/415 V delta star transformer is used in this system. The rating of LSC is selected as 3.7 kVA (maximum stator power output when the load is disconnected) and the current rating (rms) of LSC, is calculated as,

$$I_{r(LSC)} = \frac{VA_{LSC}}{\sqrt{3} \times V_{L(LV)}} = \frac{3700}{\sqrt{3} \times 125} = 17.09 \text{ A} \tag{11}$$

The current rating of each insulated gate bipolar transistor (IGBT) $I_{IGBT(LSC)}$ in LSC is obtained as,

$$I_{IGBT(LSC)} = 1.25\left\{I_{ppr} + I_{pLSC}\right\} = 31.71 \text{ A} \tag{12}$$

where, I_{ppr} is peak-peak current ripple of LSC peak current I_{pLSC} and it is considered to be 5%. So, I_{pLSC}=17.09×1.414=24.16 A and I_{ppr}=0.05×24.16=1.208 A. By substituting these values in (12), gives maximum current rating of each IGBT as 31.71 A. Therefore, a 50 A current rating IGBT is chosen.

The IGBT voltage rating depends on the DC link voltage. For example, for a 264 V as a maximum DC link voltage, the IGBT voltage rating would be 1.25×264=330 V. Here a safety margin of 25% is considered. So, a 600 V is chosen as IGBT voltage rating.
The value of interfacing inductor is calculated from the following [26],

$$L_f = \frac{\sqrt{3} \times m \times V_{dcm}}{12 \times a \times f_{sw} \times I_{ppr}} = \frac{\sqrt{3} \times 1 \times 264}{12 \times 1.2 \times 10\text{ k} \times 1.208} = 2.63 \text{ mH} \tag{13}$$

where, m denotes modulation index; a represents safety factor and its typical value is 1.2 to protect IGBT from over currents during transients; f_{sw} denotes the IGBT switching frequency; V_{dcm} represents the maximum voltage of DC link. Substituting these values in (13), gives the value of 2.63 mH.

The volt ampere (VA) rating of RSC, is on the basis of maximum real and reactive powers flow via RSC. The maximum real power flows via RSC at s_{rp} as stated in subsection-C, is calculated as,

$$\left.\begin{aligned} P_{rin} &= P_{rs} + P_{rr} = P_{rr} + \frac{P_{rr}}{|s_{rp}|} = (1 + \frac{1}{|s_{rp}|})P_{rr} \\ P_{rr} &= P_{rin}\left(\frac{|s_{rp}|}{1+|s_{rp}|}\right) = 4810\left(\frac{|-0.3|}{1+|-0.3|}\right) = 1.11 \text{ kW} \end{aligned}\right\} \tag{14}$$

The control algorithm for RSC, is such that it supplies required magnetization current to DFIG. As per machine parameters, the DFIG draws a lagging reactive power of 2.5 kVAR during motoring mode. The same is supplied from the rotor side by RSC. The rated rotor reactive power Q_{rr} at maximum slip, is calculated as,

This article has been accepted for publication in a future issue of this journal, but has not been fully edited. Content may change prior to final publication. Citation information: DOI 10.1109/TSTE.2019.2898115, IEEE Transactions on Sustainable Energy

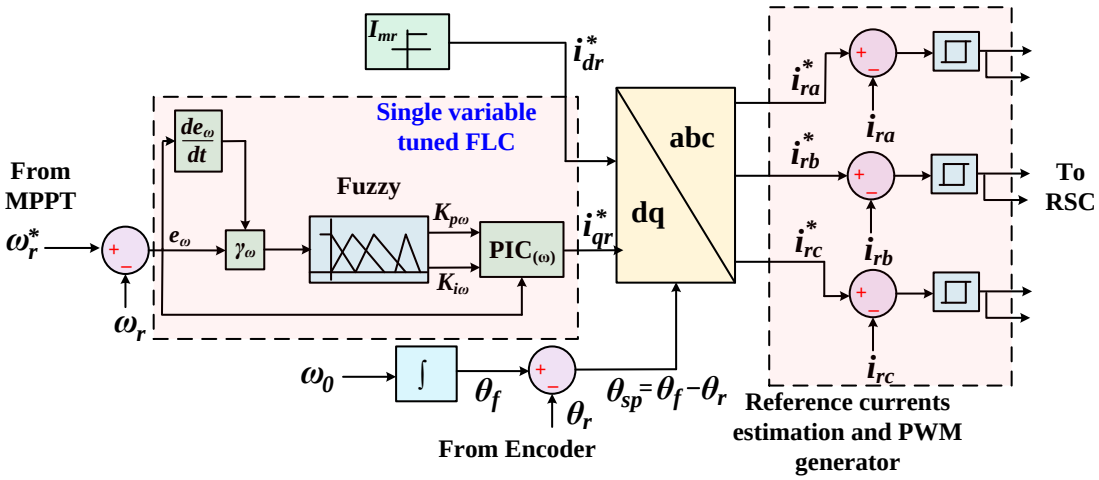

Fig. 2. Control algorithm for RSC.

$$Q_{rr} = s_{rp} \times 2.5 \text{ kVAR} = 0.75 \text{ kVAR} \quad (15)$$

Now, the overall rating of RSC is computed as,

$$VA_{(RSC)} = \sqrt{P_{rr}^2 + Q_{rr}^2} \quad (16)$$

Substituting values in (16), gives 1.34 kVA as rating of RSC. Moreover, the current rating of RSC $I_{r(RSC)}$ is computed as,

$$I_{r(RSC)} = \frac{VA_{(RSC)}}{\sqrt{3} \times V_{rm}} = \frac{1340}{\sqrt{3} \times 125} = 6.3 \text{ A} \quad (17)$$

The current rating of IGBT $I_{IGBT(RSC)}$ in RSC is calculated as,

$$I_{IGBT(RSC)} = 1.25\left\{\left(0.05 \times I_{pRSC}\right) + I_{pRSC}\right\} \quad (18)$$

where, I_{pRSC} is the peak current through the RSC, is computed as (6.3×1.414≈9 A) 9 A. Substituting these values in (18), gives 11.81 A and its value is selected as 50 A. The voltage rating is chosen similar to LSC that is 600 V.

III. Control of RSC and LSC

The control algorithms for both RSC and LSC, are discussed in these subsections. It is noted that for both RSC and LSC, an indirect current control is used and it is based on stator flux oriented approach.

A. Control Design for RSC

The most important objectives of RSC, are as follows.

- It supplies reactive power requirement of DFIG for nominal voltage generation.
- It controls the speed of the rotor to achieve MPPT operation at any wind speed conditions.

Fig. 2 depicts the control design of RSC. In stator field oriented control, the direct axis rotor current component, i_{dr} is aligned along the stator field and quadrature rotor current component i_{qr} is having phase shift of 90° with respect to i_{dr}. Therefore, i_{dr} represents reactive rotor current component and i_{qr} represents real or torque part of the rotor current. The expression for the torque, is written as,

$$T_e = \left(\frac{3}{2}\right)\left(\frac{p}{2}\right)\phi_{sd} i_{qr} \quad (19)$$

where, ϕ_{sd} denotes the stator flux; p represents number of poles of DFIG.

Because in field oriented approach, ϕ_{sd} is held constant, the q component of rotor current i_{qr}, is directly related the torque. Hence, the rotor speed of DFIG is controlled by suitably generating reference for i_{qr}. The reference speed from MPPT and actual speed, are compared and then the speed error e_ω is applied to PIC of speed PIC$_{(\omega)}$ and also to the novel single variable tuned FLC block, as shown in Fig. 2. This block is used to tune $K_{p\omega}$ and $K_{i\omega}$ for PIC of speed.

The PIC is used to track the reference speed for the rotor of DFIG. In a conventional FLC, two input variables are required to execute the output gains. The more linguistic variables in FLC, lead to increase in computational burden, memory requirement and complexity of the real-time implementation. Moreover, the FLC with two input variables, has a two dimensional fuzzy based rule whereas single input variable FLC has one dimensional fuzzy rule. Therefore, a FLC fed by

TABLE I
FUZZY RULE FOR ERROR DISTANCE OF SPEED

	Z_{-2}	Z_{-1}	Z_0	Z_{+1}	Z_{+2}
γ_ω	NH	NL	S	PL	PH

TABLE II
FUZZY RULE FOR OUTPUT GAINS

	Z_{-2}	Z_{-1}	Z_0	Z_{+1}	Z_{+2}
$K_{p\omega}$	$H_{p\omega}$	$M_{p\omega}$	$S_{p\omega}$	$M_{p\omega}$	$H_{p\omega}$
$K_{i\omega}$	$H_{i\omega}$	$M_{i\omega}$	$S_{i\omega}$	$M_{i\omega}$	$H_{i\omega}$

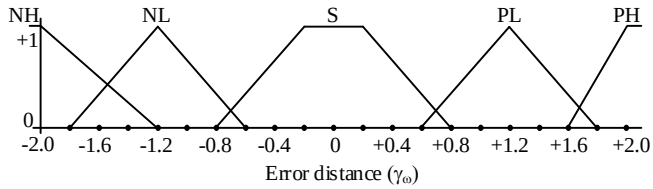

Fig. 3. Input membership function γ_ω.

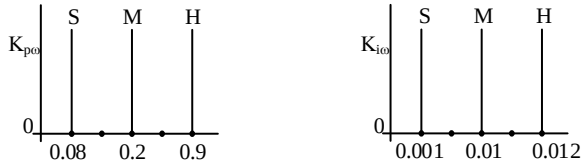

Fig. 4. Output membership functions $K_{p\omega}$, $K_{i\omega}$.

This article has been accepted for publication in a future issue of this journal, but has not been fully edited. Content may change prior to final publication. Citation information: DOI 10.1109/TSTE.2019.2898115, IEEE Transactions on Sustainable Energy

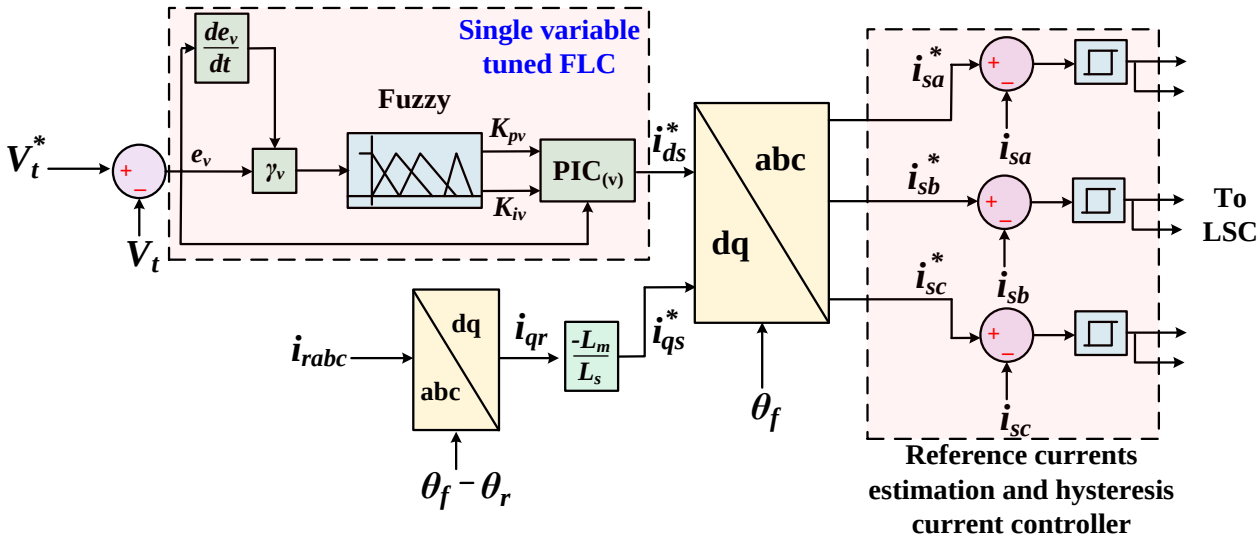

Fig. 5. Control algorithm for LSC.

single input variable is introduced. The fundamental objective of this single input variable FLC is that it generates proper proportional and integral gains as the error varies. Hence, this function eventually improves the dynamic performance especially in achieving MPPT in variable wind speed conditions. The speed error e_ω and its rate of change (de_ω/dt), are applied as inputs to the error distance γ_ω. This error distance is given as input to the FLC. The error distance is expressed in terms of error coordinates (e_ω, $e_{r\omega}$). Here, $e_{r\omega}$ denotes the rate of change of error, the error distance for speed control is estimated as,

$$\gamma_\omega = \sqrt{e_\omega^2 + e_{r\omega}^2} \tag{20}$$

The Takagi-Sugeno FLC is used here to provide gains, to properly track the reference speed of DFIG by eliminating its error with respect to actual speed. Table I and Table II provide the fuzzy rules for input and output variables, individually. Here *Z* denotes the linguistic value of γ_ω. The negative high (NH), negative low (NL), small (S), positive low (PL) and positive high (PH), are the values of error distance. Small (S), medium (M) and high (H), are the values of $K_{p\omega}$ and $K_{i\omega}$. Fig. 3 and Fig. 4 represent the membership functions of input and output, respectively. The tuned proportional and integral gains, are applied to PIC of speed to generate reference *q* component of rotor i^*_{qr} as depicted in Fig. 2, is computed as,

$$i^*_{qr(j)} = i^*_{qr(j-1)} + K_{p\omega}(e_{\omega(j)} - e_{\omega(j-1)}) + K_{i\omega} e_{\omega(j)} \tag{21}$$

where, $e_\omega = \omega^*_r - \omega_r$.

The *d* component of rotor reference current [15] is as,

$$i^*_{dr} = I_{mr} = \sqrt{\frac{2}{3}}\left[\frac{V_t}{X_m}\right] \tag{22}$$

where, I_{mr} is the magnetizing component of DFIG; X_m is the magnetizing reactance of the machine at base frequency and V_t is the terminal voltage.

These reference *dq* components are transformed in to *abc* coordinates through inverse Park transformation by means of angle of transformation θ_{sp}. The slip angle is computed from the sensed rotor angle θ_r and fixed electrical angle θ_f at base frequency ω_0 in (rad/s) as,

$$\theta_{sp} = \theta_f - \theta_r \tag{23}$$

here, $\theta_f = \int_0^t \omega_0 dt$

The estimated rotor reference currents i^*_{ra}, i^*_{rb}, and i^*_{rc} are compared with sensed currents of rotor i_{ra}, i_{rb} and i_{rc}, then error is applied to pulse width modulated control to produce pulses for the IGBT devices of RSC.

B. Control Design for LSC

The main objectives of LSC are as follows.

- It maintains constant terminal voltage at PCC by voltage control.
- It supports constant frequency by using fixed electrical angle as transformation angle.

Fig. 5 depicts the control technique of LSC. In LSC control, the reference currents are generated for the stator currents of DFIG. The reactive reference part of stator current i^*_{ds}, is estimated by passing terminal voltage error through PIC of voltage $PIC_{(V)}$ as shown in Fig. 5. In this control, gains of PIC are tuned using single input variable FLC as discussed in subsection-A. The membership functions of input and output to track voltage reference, are given in Fig. 6 and Fig. 7,

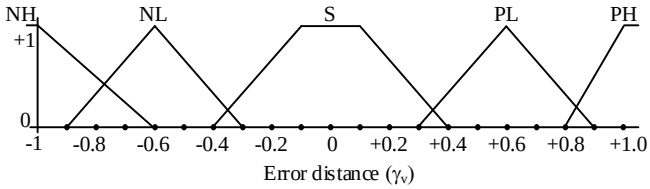

Fig. 6. Input membership function γ_v.

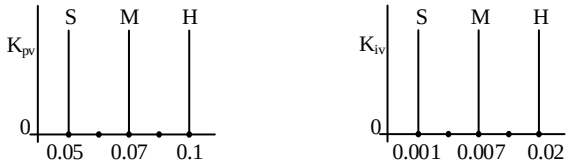

Fig. 7. Output membership functions K_{pv}, K_{iv}.

This article has been accepted for publication in a future issue of this journal, but has not been fully edited. Content may change prior to final publication. Citation information: DOI 10.1109/TSTE.2019.2898115, IEEE Transactions on Sustainable Energy

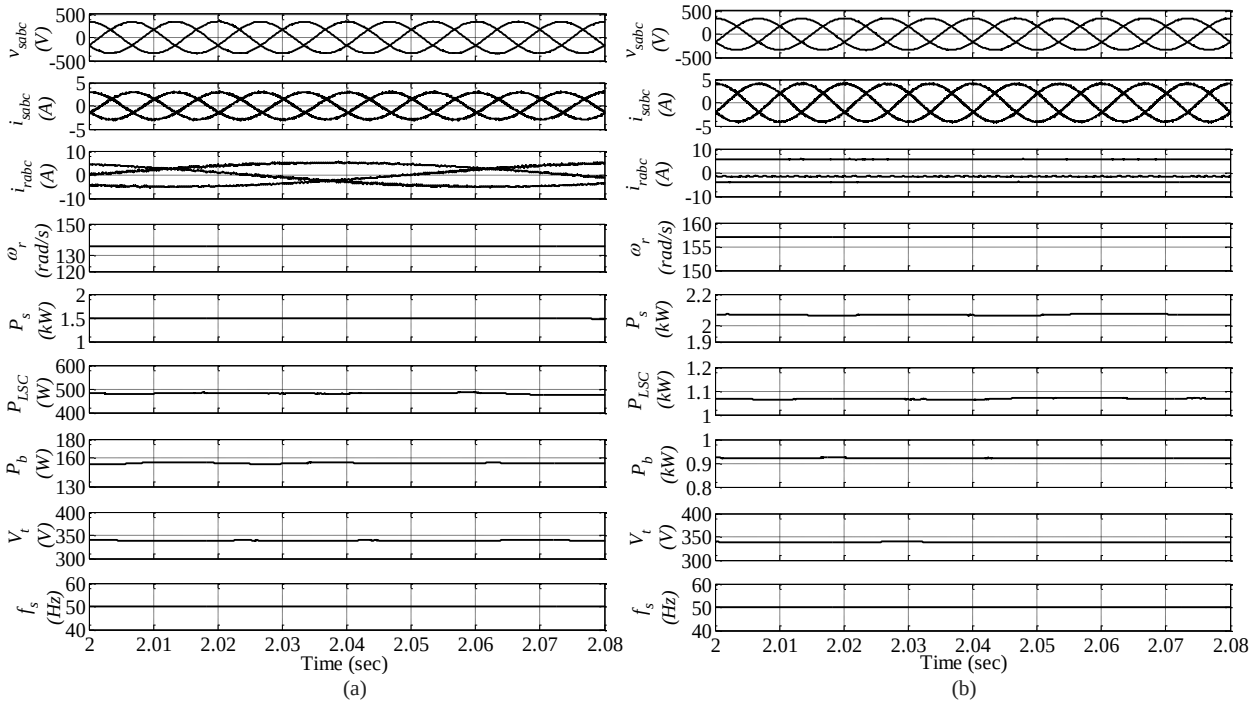

Fig. 8. Performance of the DFIG based WPGS with BES at constant wind speed of (a) 8 m/s (subsynchronous speed of DFIG): v_{sabc}, i_{sabc}, i_{rabc}, ω_r, P_s, P_{LSC}, P_b, V_t, f_s (b) 9.23 m/s (synchronous speed of DFIG): v_{sabc}, i_{sabc}, i_{rabc}, ω_r, P_s, P_{LSC}, P_b, V_t, f_s.

individually. The fuzzy rules are similar to the subsection-A. It is noted that γ_v represents the error distance, e_v denotes voltage error and (de_v/dt) indicates rate of voltage error. The tuned K_{pv} and K_{iv} are given to the FLC, which produces i^*_{ds} as,

$$i^*_{ds(j)} = i^*_{ds(j-1)} + K_{pv}(e_{v(j)} - e_{v(j-1)}) + K_{iv}e_{v(j)} \quad (24)$$

where, $e_v = V^*_t - V_t$.

The active reference part of stator current i^*_{qs} is related with the i_{qr} as follows.

$$i^*_{qs(j)} = -\left(\frac{L_m}{L_s}\right) i_{qr(j)} \quad (25)$$

The computed *dq* stator reference currents are converted back to actual *abc* coordinates by making use of inverse Park transformation with fixed electrical angle as transformation angle, which can be seen from Fig. 5. The reference stator currents i^*_{sa}, i^*_{sb}, and i^*_{sc} are brought in comparison to sensed stator winding currents i_{sa}, i_{sb} and i_{sc}, then the current error is applied to the hysteresis band current control, which produces pulses for IGBT devices within the LSC.

IV. Simulation Results

The DFIG based WPGS along with BES, is simulated using SimPowerSystems toolbox of MATLAB. The system performance is analyzed during constant wind speeds, variable wind speeds over a wide range, nonlinear load unbalancing conditions. In each scenario, the frequency and voltages are maintained at fixed value and also the voltage and current harmonics distortions are maintained as per the IEEE 519 standard. The various signals that are used in this system, are stator voltages (v_{sabc}), stator currents (i_{sabc}), rotor currents (i_{rabc}), frequency of stator (f_s), terminal voltage (V_t), optimal tip speed ratio (λ^*), rotor speed of DFIG (ω_r), turbine rotor power coefficient (C_p), stator power (P_s), LSC power (P_{LSC}), load power (P_L), battery power (P_b) and load currents (i_{Labc}).

A. Performance of System at Constant Wind Speed

The steady state responses of the DFIG based WPGS at wind speed of 8 m/s and 9.23 m/s, are depicted in Figs. 8 (a-b). It is to be noted that wind speed of 8 m/s and 9.23 m/s, are correspond to subsynchronous and synchronous speed of DFIG, respectively. Figs. 8 (a-b) demonstrate the waveforms of v_{sabc}, i_{sabc}, i_{rabc}, ω_r, P_s, P_{LSC}, P_b, V_t and f_s. In this case, a linear load of 1 kW is connected at PCC. At a wind speed of 8 m/s, the generation is more than the connected load, therefore, the remaining power flows to the battery for charging through LSC. This is observed from the waveforms of P_{LSC} and P_b, as shown in Fig. 8(a). Moreover, it is noted that the frequency and terminal voltage, are maintained at constant value. The stator voltages and currents are sinusoidal and their THDs are within the IEEE 519 standard. From the rotor currents, it is seen that the frequency of the rotor, is slip times the stator frequency. In similar lines, the rotor currents are DC at synchronous speed, as depicted in Fig. 8 (b). Here also, the battery charges, as the generation is more than the demand.

Figs. 9 (a-b) illustrate the waveforms of v_{sabc}, i_{sabc}, i_{rabc}, ω_r, P_s, P_{LSC}, P_b, V_t and f_s at wind speeds of 10 m/s and 12 m/s, respectively. Both wind speeds are correspond to supersynchronous speed region of DFIG. In both cases, the battery charges and also the terminal voltage and frequency, are maintained at constant value. It is observed that stator generates the rated power of nearly 3.7 kW at rated wind speed of 12 m/s, as depicted in Fig. 9 (b). Moreover, the stator voltages and stator currents, are sinusoidal and balanced as per the IEEE 519 standard.

B. Dynamic Response of System at Variable Wind Speed

The dynamic response of the system for wide span of wind

This article has been accepted for publication in a future issue of this journal, but has not been fully edited. Content may change prior to final publication. Citation information: DOI 10.1109/TSTE.2019.2898115, IEEE Transactions on Sustainable Energy

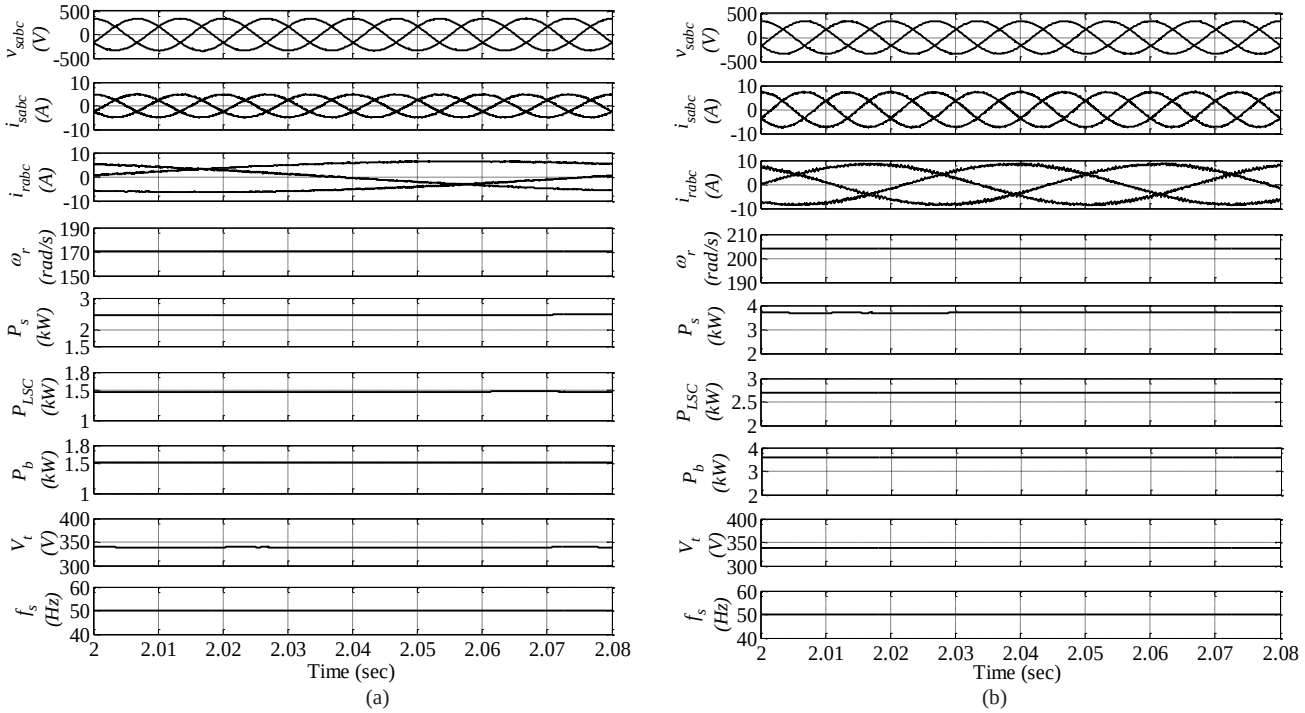

Fig. 9. Performance of the DFIG based WPGS with BES at constant wind speed of (a) 10 m/s (supersynchronous speed of DFIG): v_{sabc}, i_{sabc}, i_{rabc}, ω_r, P_s, P_{LSC}, P_b, V_t, f_s (b) 12 m/s (supersynchronous speed of DFIG): v_{sabc}, i_{sabc}, i_{rabc}, ω_r, P_s, P_{LSC}, P_b, V_t, f_s.

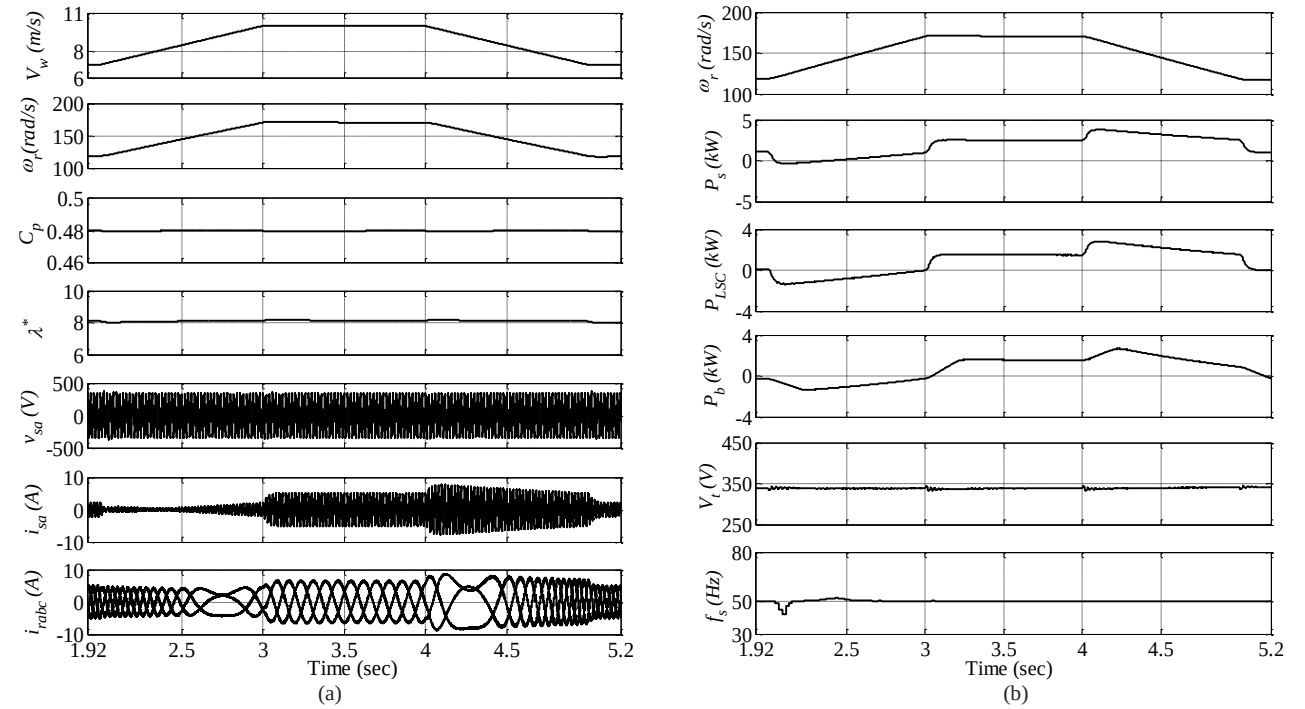

Fig. 10. Dynamic performance of DFIG based WPGS with BES for wide span of wind speed variation (a) V_w, ω_r, C_p, λ^*, v_{sa}, i_{sa}, i_{rabc} (b) ω_r, P_s, P_{LSC}, P_b, V_t, f_s.

speed variation, is depicted in Figs. 10 (a-b). Fig. 10 (a) shows the waveforms of V_w, ω_r, C_p, λ^*, v_{sa}, i_{sa}, i_{rabc}. Initially, the wind speed is kept at 7 m/s and it is raised to 10 m/s at 3 s and again it is reduced to 7 m/s at 5 s, as depicted in Fig. 10 (a). It is noted that the rotor speed follows the same pattern of wind speed variation and moreover, the values of C_p and λ^*, are almost constant, which indicates the MPPT operation of a wind turbine coupled DFIG. The dynamic response of v_{sa}, i_{sa} and i_{rabc} with change in wind speed, is depicted in Fig. 10 (a). The frequency and terminal voltage, are retained constant throughout the wind speed variation as depicted in Fig. 10 (b). Fig. 10 (b) depicts the waveforms of ω_r, P_s, P_{LSC}, P_b, V_t and f_s for the wind speed pattern shown in Fig. 10 (a). Initially, the battery discharges and supplies the remaining load as the generation is less than the connected load. As the wind speed increases, the battery is charged. This is evident from the waveforms of P_s, P_{LSC} and P_b. Moreover, the THDs of voltages and currents are found within the IEEE 519 standard for the entire span of wind speed variation.

This article has been accepted for publication in a future issue of this journal, but has not been fully edited. Content may change prior to final publication. Citation information: DOI 10.1109/TSTE.2019.2898115, IEEE Transactions on Sustainable Energy

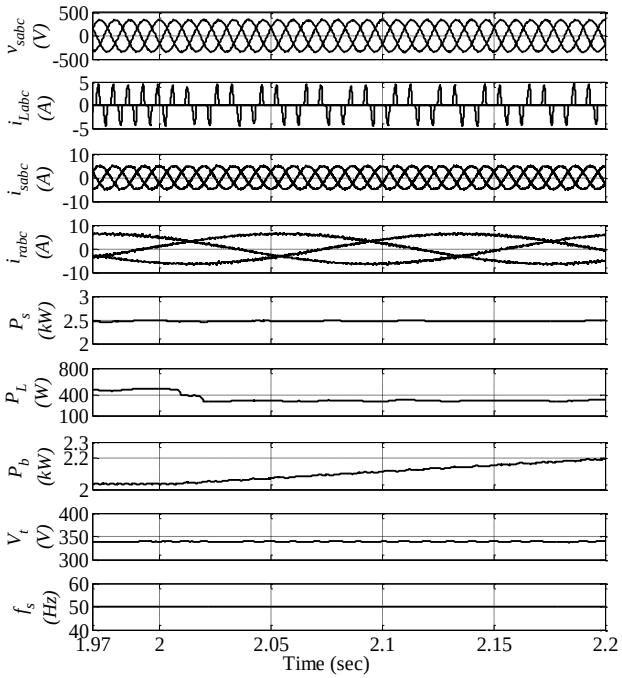

Fig. 11. Dynamic response of the system for nonlinear unbalancing load : v_{sabc}, i_{Labc}, i_{sabc}, i_{rabc}, P_s, P_L, P_b, V_t, f_s.

C. Performance of System at Nonlinear Load Unbalancing

Fig. 11 shows the dynamic performance of a system during nonlinear load unbalancing at a wind speed of 10 m/s. The nonlinear load is realized by connecting three single phase diode bridge rectifiers (DBRs) with resistor and capacitor connected in parallel at DC side of DBR. Fig. 11 shows the waveforms of v_{sabc}, i_{Labc}, i_{sabc}, i_{rabc}, P_s, P_L, P_b, V_t and f_s. Initially, a balanced nonlinear load is connected and phase 'a' is disconnected at 2 s to create load unbalance, as depicted in Fig. 11. Since the wind speed is constant, the decreased load power flows to the BES and increases the battery power, as depicted in Fig. 11. The DFIG stator currents and voltages, are found sinusoidal and balanced even under load unbalancing. Moreover, the terminal voltage and frequency, are retained at the same value.

V. Hardware Implementation

To validate the proposed DFIG based WPGS in standalone mode with a novel control scheme, a prototype of 3.7 kW DFIG is developed in the laboratory. A wound rotor induction machine is used as a DFIG. The wind turbine characteristics are emulated using a buck chopper and separately excited DC shunt motor. The field winding voltage applied to the DC shunt motor is kept constant and hence the torque is controlled by proper control of armature current. To achieve 240 V at the DC link, a battery bank, which has 40 numbers of 12 V, 7 AH, are connected in two parallel circuits. Two 3-phase VSCs are used as a RSC and LSC of DFIG and stator windings straightaway feed the load. The PCC voltages, (v_{ab},v_{bc}) are sensed by using Hall-Effect voltage sensors and load currents (i_{Labc}), stator currents (i_{sabc}), LSC currents (i_{LSC}) and rotor winding currents (i_{rabc}) are sensed using Hall-Effect current sensors. The digital signal processor (dSPACE-1103 R&D digital controller) at a sampling time of 35 μs is used to implement the control technique for both RSC and LSC, in order to provide pulses for IGBT devices. The steady state waveforms are captured using power quality analyzer (Fluke 43-B). Some of the steady state and dynamic waveforms are taken using digital storage oscilloscope. The detailed parameters of experimental prototype are given in Appendices. A photograph of the experimental prototype of DFIG based standalone WPGS, is demonstrated in Fig. 12. The detailed description of various components are illustrated in Fig. 12. For better clarity, the zoom view of the BES is also depicted in Fig. 12.

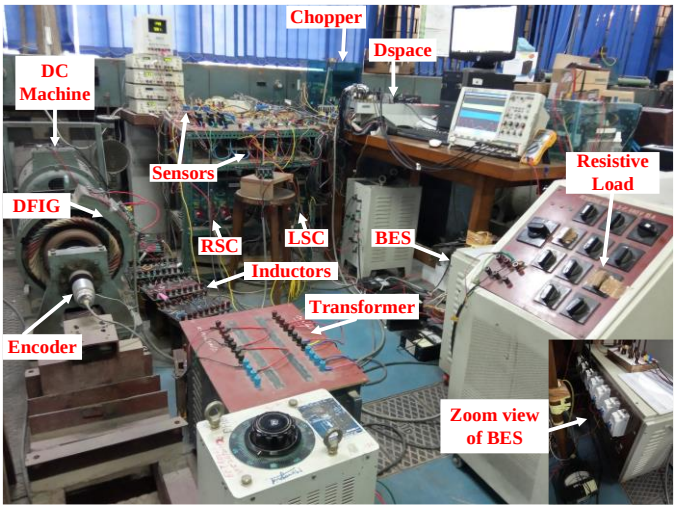

Fig. 12. View of experimental prototype.

A. Performance of System at Nonlinear Load

Figs. 13 (a-j) depict the steady state results of the system at nonlinear load connected at PCC. Figs. 13 (a-c) show the voltage and current waveforms of stator, load and LSC. Figs. 13 (d-f) show the power of stator, load and LSC. Here the generation is more than the demand, so the excess power goes through the LSC and charges the battery. This is recognized by the negative sign of LSC power. Figs. 13 (g-i) show the

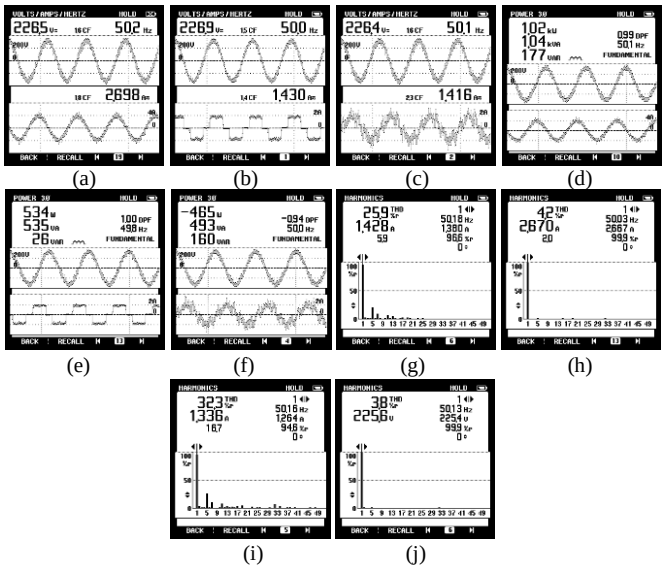

Fig. 13. Experimental waveforms of a system at steady state with nonlinear load (a-c) voltage and current waveforms of stator, load and LSC (d-f) stator power, load power, LSC power (g-i) harmonic spectrum of load, stator and LSC current (j) harmonic spectrum of PCC voltage.

This article has been accepted for publication in a future issue of this journal, but has not been fully edited. Content may change prior to final publication. Citation information: DOI 10.1109/TSTE.2019.2898115, IEEE Transactions on Sustainable Energy

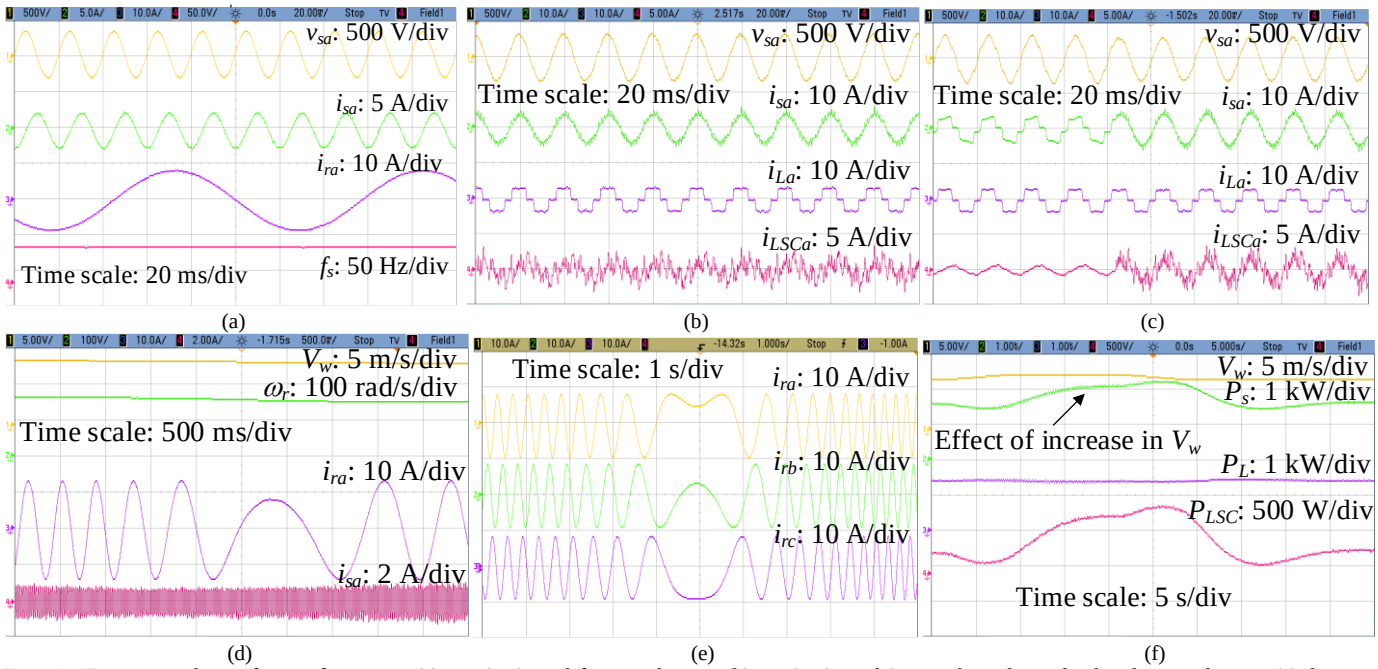

Fig. 14. Experimental waveforms of a system (a) v_{sa}, i_{sa}, i_{ra} and f_s at steady state (b) v_{sa}, i_{sa}, i_{La} and i_{LSCa} with nonlinear load and at steady state (c) dynamic response of v_{sa}, i_{sa}, i_{La} and i_{LSCa} with nonlinear load (d) dynamic response during variable wind speed: V_w, ω_r, i_{ra} and i_{sa} (e) dynamic response of rotor currents when speed changes from sub-synchronous to super-synchronous speed: i_{ra}, i_{rb} and i_{rc} (f) power variation at variable wind speed: V_w, P_s, P_L and P_{LSC}.

current THD of load, stator and LSC. The load current THD is 25.9%, but when LSC is switched on then stator current THD becomes 4.2%, which is within the IEEE 519 standard. Fig. 13 (j) shows the voltage THD at PCC, which is also found well within the IEEE 519 standard.

B. Performance of System at Variable Wind Speed

Fig. 14 (a) depicts the steady state waveforms of stator voltage, stator current, rotor current and stator frequency. It is evident from these results that the stator frequency is maintained at constant value of 50 Hz and rotor current frequency is slip times the stator frequency. Fig. 14 (b) demonstrates the waveforms of v_{sa}, i_{sa}, i_{La} and i_{LSCa} at nonlinear load. The stator current becomes sinusoidal because the load harmonics are supplied by the LSC as shown in Fig. 14 (b). Fig. 14 (c) shows the waveforms of v_{sa}, i_{sa}, i_{La} and i_{LSCa} at nonlinear load, before and after LSC comes in to operation. When LSC is turned off, the stator and load currents are the same, but after LSC is turned on, the voltage and current of stator, become sinusoidal. This clearly represents the LSC behavior as an active shunt filter. Fig. 14 (d) shows the response of system when the rotor speed changes from super-synchronous to sub-synchronous as wind speed changes. Fig. 14 (d) shows the waveforms of wind speed, rotor speed, rotor and stator winding currents. With a decrease in wind speed, the speed of the rotor also falls. The pattern of rotor current clearly shows the transition of DFIG operation from super-synchronous to sub-synchronous speed. The same observation is clearly visible in Fig. 14 (e), where all three phase rotor currents are captured during rotor speed changes from sub-synchronous to super-synchronous speed. Fig. 14 (f) demonstrates the waveforms of wind speed, stator power, load power and LSC power. As wind speed increases, the stator power also increases. Since the load is constant, the remaining extra power goes to the battery via LSC. This is clearly evident from the LSC power variation along with stator power variation as shown in Fig. 14 (f).

In order to show the robustness of the developed prototype, the experimental results are shown for wide span of wind speed variation. Figs. 15 (a-f) depict the dynamic response of system at variable wind speeds over a wide range. Fig. 15 (a) depicts the waveforms of V_w, ω_r, P_s and i_{ra} for change in wind speed over wide range. As the wind speed increases, the rotor speed is increased. This shows the wind MPPT operation of DFIG. The response of stator power and rotor current, is also depicted. The rotor current depicts the multiple times transition of rotor speed from subsynchronous to supersynchronous speed region and vice versa. Figs. 15 (b-c) demonstrate the waveforms of ω_r, v_{sa}, i_{sa} and i_{ra} for an increase and a decrease in wind speeds, respectively. Fig. 15 (d) depicts the waveforms of V_w, ω_r, V_t and f_s for change in wind speed pattern. Moreover, Fig. 15 (e) depicts the waveforms of ω_r, i_{ra}, V_t and f_s for change in wind speed. It is noted that a small dip in terminal voltage occurs. However, it is restored quickly to the normal value as seen from Fig. 15 (e). Fig. 15 (f) illustrates the waveforms of V_w, P_s, i_{ra} and P_b. Since the connected load is constant, the increase in stator power due to increase in wind speed flows to the battery for charging. This is clearly viewed from P_b of Fig. 15 (f). Moreover, the frequency of rotor current during subsynchronous speed ($\omega_r<\omega_s$), synchronous speed ($\omega_r=\omega_s$) and supersynchronous speed ($\omega_r>\omega_s$), is evident from i_{ra}.

VI. Conclusion

A novel single input variable FLC based control has been proposed for DFIG based WPGS in standalone mode. This novel FLC is used to tune proportional and integral controllers gains according to the error dynamics such that MPPT is

This article has been accepted for publication in a future issue of this journal, but has not been fully edited. Content may change prior to final publication. Citation information: DOI 10.1109/TSTE.2019.2898115, IEEE Transactions on Sustainable Energy

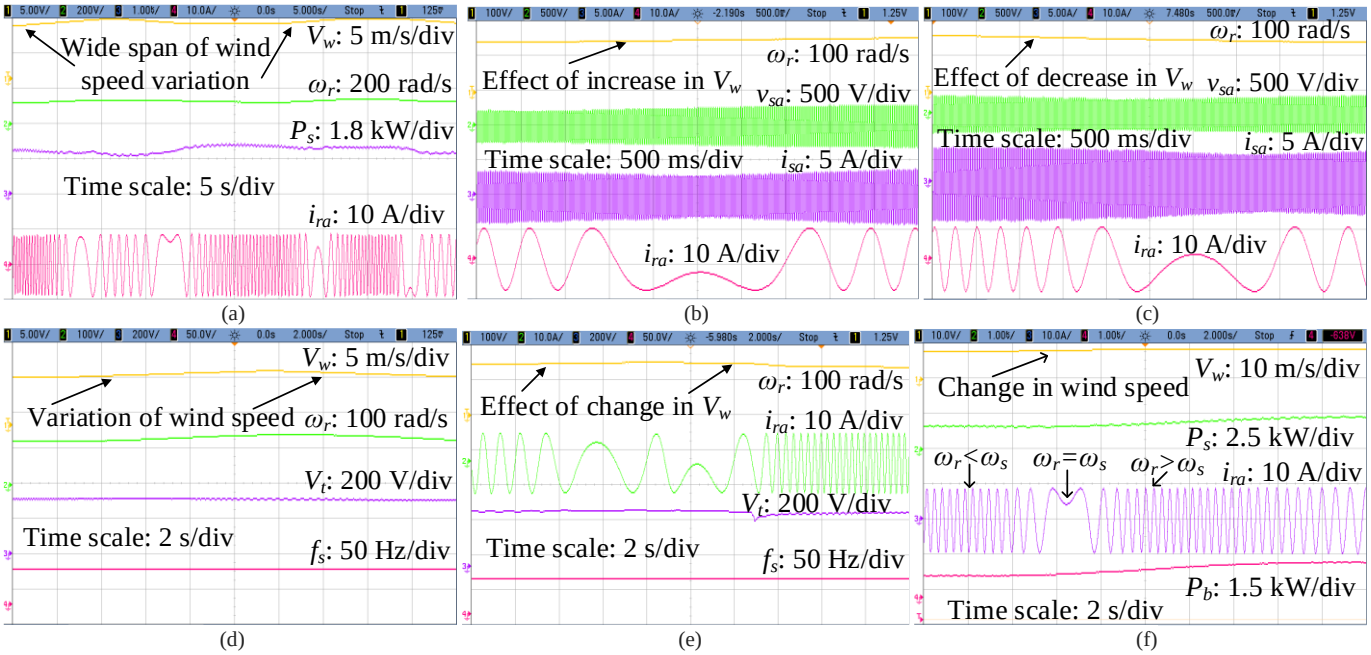

Fig. 15. Experimental performance of system for wide span of wind speed variation (a) V_w, ω_r, P_s, i_{ra} (b) at increase in wind speed: ω_r, v_{sa}, i_{sa}, i_{ra} (c) at decrease in wind speed: ω_r, v_{sa}, i_{sa}, i_{ra} (d) V_w, ω_r, V_t, f_s (e) ω_r, i_{ra}, V_t, f_s (f) V_w, P_s, i_{ra}, P_b.

tracked efficiently even under dynamic operating conditions. The BES has been used to store the surplus energy, when the load demand is less than the generation and also to supply the balance power, when the load demand is more than the generation. The significant achievements using proposed control scheme, are highlighted as follows.

- The stator voltages and currents are sinusoidal and balanced even under presence of nonlinear and unbalanced load conditions.
- The extraction of maximum power from the variable wind speed is effectively achieved under low and wide span of wind speed variation.
- The terminal voltage and frequency of the DFIG based WPGS, are maintained constant irrespective of wind speed variations.

Simulated results show that the system works satisfactorily at variable wind speeds and also at nonlinear load unbalancing. The total harmonic distortions of stator voltages and stator currents, are found within the IEEE 519 standard. Moreover, experimental results have shown the satisfactory performance of the presented system.

ACKNOWLEDGMENTS

The authors are extremely grateful to DST, GoI (Grant Number: RP03391 (UKICERI)), and J. C. Bose Fellowship (Grant Number: RP03128) for their financial assistance to this work.

APPENDICES

A. Parameters of DFIG (Simulation and Experimental)

Make- McFEC Ltd, Rating: 3.7 kW, 400 V, 50 Hz, 4 Pole, stator windings connection-Y, R_s = 1.32 Ω, R_r=1.708 Ω, L_m = 219 mH, L_{ls} = 6.832 mH, L_{lr} = 6.832 mH, Inertia = 0.1878 kg-m^2.

REFERENCES

[1] M. Marchi, V. Niccolucci, R. M. Pulselli, and N. Marchettini, "Environmental policies for GHG emissions reduction and energy transition in the medieval historic centre of Siena (Italy): the role of solar energy," *Journal of Cleaner Production*, vol. 185, pp. 829-840, 2018.

[2] P. Haan, M. Simmler, "Wind electricity subsidies-A windfall for landowners? Evidence from a feed-in tariff in Germany," *Journal of Public Economics*, vol. 159, pp. 16-32, 2018.

[3] W. Li, P. Chao, X. Liang, J. Ma, D. Xu, and X. Jin, "A practical equivalent method for DFIG wind farms," *IEEE Trans. Sustain. Energy*, vol. 9, no. 2, pp. 610-620, Sept. 2018.

[4] T. Malakar, S.K. Goswami, and A.K. Sinha, "Impact of load management on the energy management strategy of a wind-short hydro hybrid system in frequency based pricing," *Energy Convers. and Manage*., vol 79, pp. 200-212, March 2014.

[5] V. Gholamrezaie, M. G. Dozein, H. Monsef, and B. Wu, "An optimal frequency control method through a dynamic load frequency control (LFC) model incorporating wind farm," *IEEE Systems Journal*, vol. 12, no. 1, pp. 392-401, March 2018.

[6] H. Li and Z. Chen, "Overview of different wind generator systems and their comparisons," *IET Renewable Power Generation*, vol. 2, no. 2, pp. 123-138, June 2008.

[7] C. Wu and H. Nian, "Stator harmonic currents suppression for DFIG based on feed-forward regulator under distorted grid voltage," *IEEE Trans. Power Electron*., vol. 33, no. 2, pp. 1211-1224, Feb. 2018.

[8] C. Cheng and H. Nian, "Low-complexity model predictive stator current control of DFIG under harmonic grid voltages," *IEEE Trans. Energy Convers*., vol. 32, no. 3, pp. 1072-1080, Sept. 2017.

[9] D. Sun, X. Wang, H. Nian, and Z. Q. Zhu, "A sliding-mode direct power control strategy for DFIG under both balanced and unbalanced grid conditions using extended active power," *IEEE Trans. Power Electron*., vol. 33, no. 2, pp. 1313-1322, Feb. 2018.

[10] I. D. Margaris, S. A. Papathanassiou, N. D. Hatziargyriou, A. D. Hansen, and P. Sorensen, "Frequency control in autonomous power systems with high wind power penetration," *IEEE Trans. Sustain. Energy*, vol. 3, no. 2, pp. 189-199, April 2012.

[11] J. Hussain and M. K. Mishra, "Adaptive maximum power point tracking control algorithm for wind energy conversion systems," *IEEE Trans. Energy Convers*., vol. 31, no. 2, pp. 697-705, June 2016.

[12] J. Tian, D. Zhou, C. Su, Z. Chen, and F. Blaabjerg, "Reactive power dispatch method in wind farms to improve the lifetime of power

converter considering wake effect," *IEEE Trans. Sustain. Energy*, vol. 8, no. 2, pp. 477-487, April 2017.

[13] N. Mendis, K. M. Muttaqi, S. Sayeef, and S. Perera, "Standalone operation of wind turbine-based variable speed generators with maximum power extraction capability," *IEEE Trans. Energy Convers.*, vol. 27, no. 4, pp. 822-834, Dec. 2012.

[14] R. Cardenas, R. Pena, J. Proboste, G. Asher, and J. Clare, "MRAS observer for sensorless control of standalone doubly fed induction generators," *IEEE Trans. Energy Convers*., vol. 20, no. 4, pp. 710-718, Dec. 2005.

[15] P. K. Goel, B. Singh, S. S. Murthy, and N. Kishore, "Modeling and control of autonomous wind energy conversion system with doubly fed induction generator," in *Proc. Joint International Conference on Power Electronics, Drives and Energy Systems & 2010 Power India*, New Delhi, 2010, pp. 1-8.

[16] N. K. Swami Naidu and B. Singh, "Experimental implementation of doubly fed induction generator-based standalone wind energy conversion system," *IEEE Trans. Ind. Applicat*., vol. 52, no. 4, pp. 3332-3339, July-Aug. 2016.

[17] S. Demirbas, "Self-tuning fuzzy-PI-based current control algorithm for doubly fed induction generator," *IET Renewable Power Generation*, vol. 11, no. 13, pp. 1714-1722, Nov. 2017.

[18] S. Krishnama Raju and G. N. Pillai, "Design and implementation of type-2 fuzzy logic controller for DFIG-based wind energy systems in distribution networks," *IEEE Trans. Sustain. Energy*, vol. 7, no. 1, pp. 345-353, Jan. 2016.

[19] Byung-Jae Choi, Seong-Woo Kwak, and Byung Kook Kim, "Design of a single-input fuzzy logic controller and its properties," *Fuzzy Sets and Systems*,vol. 106, no. 3,pp. 299-308, 1999.

[20] Peng Seng Toh, Multiple energy harvester to power standalone electrical appliances, WO2006022590A1, 2006.

[21] Q. Wu, E. Larsen, K. Heussen, H. Binder, and P. Douglass, "Remote off-grid solutions for greenland and denmark: Using smart-grid technologies to ensure secure, reliable energy for island power systems," *IEEE Electrification Magazine*, vol. 5, no. 2, pp. 64-73, June 2017.

[22] L. Guo, Z. Yu, C. Wang, F. Li, .J Schiettekatte, J. Deslauriers, and L. Bai, "Optimal design of battery energy storage system for a wind–diesel off-grid power system in a remote canadian community," *IET Generation, Transmission & Distribution*, vol. 10, no. 3, pp. 608-616, Feb. 2016.

[23] J. Grainger and W. Stevenson, *Power System Analysis*. McGraw Hill Education; 1st edition, July 2017.

[24] D. P. Kothari, I. Nagrath, *Modern Power System Analysis*. McGraw Hill Education; 4th edition, June 2011.

[25] B. Singh and G. K. Kasal, "Voltage and frequency controller for a three-phase four-wire autonomous wind energy conversion system," *IEEE Trans. Energy Convers.*, vol. 23, no. 2, pp. 509-518, June 2008.

[26] Bhim Singh, Ambrish Chandra, and Kamal Al-Haddad, *Power Quality: Problems and Mitigation Techniques*. West Sussex, U.K.: Wiley, 2015.

Sambasivaiah Puchalapalli (S'16, M'19) was born in SPSR Nellore, Andhra Pradesh, India, in 1992. He received the B.Tech. degree in Electrical and Electronics Engineering from N.B.K.R. Institute of Science and Technology, Vidyanagar, Andhra Pradesh, India and the M.Tech. degree in Electrical Engineering from the Indian Institute of Technology Gandhinagar (IITGN), Palaj, India, in 2013 and 2016, respectively. He is currently working toward the Ph.D. degree at the Department of Electrical Engineering, Indian Institute of Technology Delhi (IITD), New Delhi, India.

His research interests include doubly fed induction generator (DFIG) based wind energy conversion systems, solar energy conversion systems, power quality improvement in the distribution systems, and microgrid-based power systems.

Mr. Sambasivaiah was the recipient of the Institute Gold Medal in M.Tech. Electrical Engineering (2016), Indian Institute of Technology Gandhinagar.

Bhim Singh (SM'99, F'10) was born in Rahamapur, Bijnor (UP), India, in 1956. He has received his B.E. (Electrical) from the University of Roorkee (Now IIT Roorkee), India, in 1977 and his M.Tech. (Power Apparatus & Systems) and Ph.D. from the Indian Institute of Technology Delhi, India, in 1979 and 1983, respectively.

In 1983, he joined the Department of Electrical Engineering, University of Roorkee, as a Lecturer. He became a Reader there in 1988. In December 1990, he joined the Department of Electrical Engineering, IIT Delhi, India, as an Assistant Professor, where he has become an Associate Professor in 1994 and a Professor in 1997. He has been ABB Chair Professor from September 2007 to September 2012. He has also been CEA Chair Professor from October 2012 to September 2017. He has been Head of the Department of Electrical Engineering at IIT Delhi from July 2014 to August 2016. Since, August 2016, he is the Dean, Academics at IIT Delhi. He is JC Bose Fellow of DST, Government of India since December 2015. Prof. Singh is the Chairman of BOG, Maulana Azad National Institute of Technology, Bhopal, since 3rd July 2018 for 3 Years and Non-official Independent Director, NTPC Limited, since 17th July 2018 for 3 Years. He is CEA Chair Professor since January 2019.

Prof. Singh has guided 74 Ph.D. dissertations, and 166 M.E./M.Tech./M.S.(R) theses. He has been filed 37 patents. He has executed more than eighty sponsored and consultancy projects. He has co-authored a text book on power quality: *Power Quality Problems and Mitigation Techniques* published by John Wiley & Sons Ltd. 2015.

His areas of interest include solar PV grid interface systems, microgrids, power quality monitoring and mitigation, solar PV water pumping systems, improved power quality AC-DC converters, power electronics, electrical machines, drives, flexible alternating transmission systems, and high voltage direct current systems.

Prof. Singh is a Fellow of the Indian National Academy of Engineering (FNAE), The Indian National Science Academy (FNA), The National Academy of Science, India (FNASc), The Indian Academy of Sciences, India (FASc), The World Academy of Sciences (FTWAS), Institute of Electrical and Electronics Engineers (FIEEE), the Institute of Engineering and Technology (FIET), Institution of Engineers (India) (FIE), and Institution of Electronics and Telecommunication Engineers (FIETE) and a Life Member of the Indian Society for Technical Education (ISTE), System Society of India (SSI), and National Institution of Quality and Reliability (NIQR).

He has received Khosla Research Prize of University of Roorkee in the year 1991. He is recipient of JC Bose and Bimal K Bose awards of The Institution of Electronics and Telecommunication Engineers (IETE) for his contribution in the field of Power Electronics. He is also a recipient of Maharashtra State National Award of Indian Society for Technical Education (ISTE) in recognition of his outstanding research work in the area of Power Quality. He has received PES Delhi Chapter Outstanding Engineer Award for the year 2006. Professor Singh has received Khosla National Research Award of IIT Roorkee in the year 2013. He is a recipient of Shri Om Prakash Bhasin Award-2014 in the field of Engineering including Energy & Aerospace. Professor Singh has received IEEE PES Nari Hingorani Custom Power Award-2017. He is also a recipient of "Faculty Research Award as a Most Outstanding Researcher" in the field of Engineering-2018 of Careers-360, India. He has received Sulochana & Colonel A Krishnaswami VrC VSM** Faculty Lifetime Research Award-2018 for overall research contribution at IIT Delhi.

He has been the General Chair of the 2006 IEEE International Conference on Power Electronics, Drives and Energy Systems (PEDES'2006), General Co-Chair of the 2010 IEEE International Conference on Power Electronics, Drives and Energy Systems (PEDES'2010), General Co-Chair of the 2015 IEEE International Conference (INDICON'2015), General Co-Chair of 2016 IEEE International Conference (ICPS'2016) held in New Delhi, General Co-Chair of 2017 National Power Electronics Conference (NPEC) held in Pune.

Prof. Singh has been Chair, PES-IAS Delhi Chapter for 2005-2010, (PES-IAS Delhi Chapter won Outstanding Chapter Award-2005 Large and High Performance Chapter Award Every Year). Prof. Singh has been Chair, PELS-IES Delhi Chapter 2007-2010 and Founder Chair, PELS-IES Delhi Chapter. He has been Chair of IEEE Delhi Section for 2012-2014.